Available online at www.sciencedirect.com
SCIENCE DIRECT
Cement and Concrete Research 36 (2006) 428 – 433
Cement and Concrete Research

Chemical structure of cement aged at normal and elevated temperatures and pressures, Part II: Low permeability class G oilwell cement

Gwenn Le Saoût [a,b,*], Eric Lécolier [a], Alain Rivereau [a], Hélène Zanni [b]

[a] Institut Français du Pétrole, 1–4 av de Bois Préau, 92852 Rueil-Malmaison, France
[b] Laboratoire de Physique et Mécanique des Milieux Hétérogènes UMR CNRS 7636, Ecole Supérieure de Physique et Chimie Industrielles, 10 rue Vauquelin, 75231 Paris Cedex 05, France

Received 29 November 2004; accepted 9 November 2005

Abstract

Recently, Low Permeability Cement formulation has been developed for oilwell cementing. Therefore, it is important to understand the physical and chemical processes causing cement degradation in the downhole environment. In this study, we have characterised a Low Permeability Class G oilwell Cement immersed for one year in brine at $T=293$ K, $p=10^5$ Pa and $T=353$ K, $p=7\times10^6$ Pa using ^{29}Si, ^{27}Al NMR and XRD techniques. Elevated temperature and pressure conditions increase the rate of the pozzolanic reaction and have significant effects on the polymerisation of C–S–H and on the incorporation of Al in the C–S–H structure. Leaching resulted in the formation of calcite and a more polymerised C–S–H with the appearance of tobermorite in the sample cured at elevated temperature and pressure.

Keywords: Temperature; X-ray diffraction; NMR; Aging; Oilwell cement

1. Introduction

Cement-based materials are used in oil and gas industry for oilwell cementing [1]. At the end of the production phase on mature oil or gas field, old wells should be definitively plugged. The plug procedures should respect local legislation requirements mainly focused on the quality of cementing and the durability of the cement plug. To improve plug and abandonment operations, a Low Permeability Class G cement formulation has been recently developed [2]. The main idea of this formulation is to reduce the porosity of the set material by optimising the granular size distribution of the dry blend composed of cement, sand and silica fume. After the investigation of the chemical structure of a conventional Class G formulation [3,4], the objective of this work is to investigate the chemical evolution of this low permeability cement formulation cured and stored under downhole conditions.

Nuclear Magnetic Resonance (NMR) and X-Ray Diffraction (XRD) techniques are used to examine the hydration products of Class G cement. XRD investigates the highly crystallized phases whereas NMR is very well suitable for the study of amorphous as well as crystalline materials [5]. Previous structural characterisations of this system cured 30 days in tap water at $T=293$ K, $p=10^5$ Pa and $T=353$ K, $p=7\times10^6$ Pa revealed that an increase of pressure and temperature leads to the consumption of all the portlandite released during cement hydration as a result of an increase of the pozzolanic activity of silica fume with temperature and pressure [6]. We present in this study the investigation of the chemical composition of these samples exposed to brine during one year.

2. Experimental details

Characteristics of the Low Permeability class G cement samples (labelled LPC in the text) and curing conditions are reported in Table 1. The unhydrated cement used was a Class G Portland cement from the Dyckerhoff company (Bogue composition (wt.%) : 51.2 C_3S, 27.0 C_2S, 2.3 C_3A, 14.4 C_4AF). Sand and silica fume were added to the Class G

* Corresponding author. Present address: Laboratory of Construction Materials, Ecole Polytechnique Fédérale de Lausanne (EPFL), Ecublens, 1015 Lausanne, Switzerland. Tel.: +41 21 693 2821; fax: +41 21 693 5800.
E-mail address: gwenn.lesaout@epfl.ch (G. Le Saoût).

0008-8846/$ - see front matter © 2005 Elsevier Ltd. All rights reserved.
doi:10.1016/j.cemconres.2005.11.005

Table 1
Characteristics of cement mixes (weight ratios relative to cement mass) and curing conditions

Formulations	LPC	
Components	LPC I	LPC II
Cement class G	1	
Silica fume	0.24	
Sand	0.2	
Cement dispersant	0.018	
Water	0.27	
Curing conditions	T=293 K $p=10^5$ Pa	T=353 K $p=7\times10^6$ Pa

Portland cement to increase mechanical and durability properties by optimising the material compactness [7]. The addition of silica fume produces secondary hydrates by pozzolanic reaction with the lime resulting from primary hydration ($SiO_2+Ca(OH)_2\rightarrow C-S-H$) [8]. Silica fume has a very high water demand, because of its high specific surface area, so a cement dispersant (also named superplasticizer), polynaphtalene sulfonate (PNS), was incorporated in the mixes to maintain adequate consistency at reasonable water/cement ratio. Specimens were cast in rectangular moulds ($2\times2\times30$ cm) and were hardened in slightly hard tap water (2.9×10^{-3} M $CaCO_3$) for 30 days with two curing temperature and pressure conditions: T=293 K, $p=10^5$ Pa (samples labelled LPCI in the text) and T=353 K, $p=7\times10^6$ Pa (LPCII). Specimens were demoulded and 2 cm cubes were cut from the bars before being placed in the brine, which has neutral pH and is approximately 0.35 M NaCl (chemical composition is reported in the Part I [3]) up to one year with the two curing temperature and pressure conditions. The volume ratio of the brine to the volume of the material was 10 volume brine to 1 volume cement and the brine was renewed monthly. The present conditions are used to investigate the material behaviour under the long-term action of brine in representative conditions. We avoid using demineralised water or acid solutions currently used in the leaching tests that can lead to non-representative results [9]. After one year, chemical analyses were made on the superficial layer of typically 200–300 μm thickness, which was in contact with brine and on the bulk sample. As in the previous study [3], cement paste cubes kept their integrity without any cracks or crumbling at the surface.

X-ray diffraction (XRD) data were collected using a Philips PW 1820 diffractometer employing the CuK_α radiation (λ_0=1.54 Å). The samples were scanned at 0.6° per minute between 5° and 65° 2θ.

The ^{29}Si and ^{27}Al NMR spectra were carried out on a Bruker ASX 500 spectrometer (11.7 T magnetic field) respectively at 99.3 and 130.2 MHz. ^{29}Si spectra were recorded at 5.5 kHz spinning rate in 7 mm ZrO_2 rotors. Single pulse experiments were carried out by applying 90° pulses without ^{1}H decoupling with recycle delay of 60 s in order to respect the relaxation times T_1 of the species present in the samples (T_1=0.043 s for alite, 0.41 s for belite and 12 s for silica fume) except for sand (crushed quartz). Quartz has an extremely long non-exponential relaxation delay therefore its quantitative NMR analysis is very time consuming. Subsequently, with a recycle decay of 60 s, the contribution of quartz magnetization is negligible (less than 2% of the whole spectrum). The ^{29}Si isotropic chemical shift of the peaks were analysed using the Q^n(mAl) classification where the Si tetrahedron is connected to mAl and (n−m) Si tetrahedra where n=0 to 4 and m=0 to n. The assignments of the ^{27}Al and ^{29}Si NMR peaks have been discussed in detail in Part I. The ^{27}Al NMR spectra were recorded at 25 kHz spinning rate in 2.5 mm ZrO_2 rotors. All experiments employed single pulse ($\pi/12$) excitation width pulse of τ_p=0.5 μs without ^{1}H decoupling and a 1 s relaxation delay. The ^{27}Al and ^{29}Si chemical shifts were respectively referenced relative to a 1.0 M $AlCl_3-6H_2O$ solution and to tetramethylsilane $Si(CH_3)_4$ (TMS) at 0 ppm, using $Si[(CH_3)_3]_8Si_8O_{20}$ (Q_8M_8) as a secondary reference (the major peak being at 11.6 ppm relatively to TMS).

3. Results and discussion

3.1. X-ray diffraction

Figs. 1 and 2 show the XRD patterns of samples cured respectively at ambient temperature and atmospheric pressure (LPCI) and at T=353 K and $p=7\times10^6$ Pa (LPCII) for 30 days and one year. XRD results show little variation in mineralogy with temperature and pressure conditions and curing time in LPC samples. Unhydrated phases alite C_3S, belite C_2S, ferrite

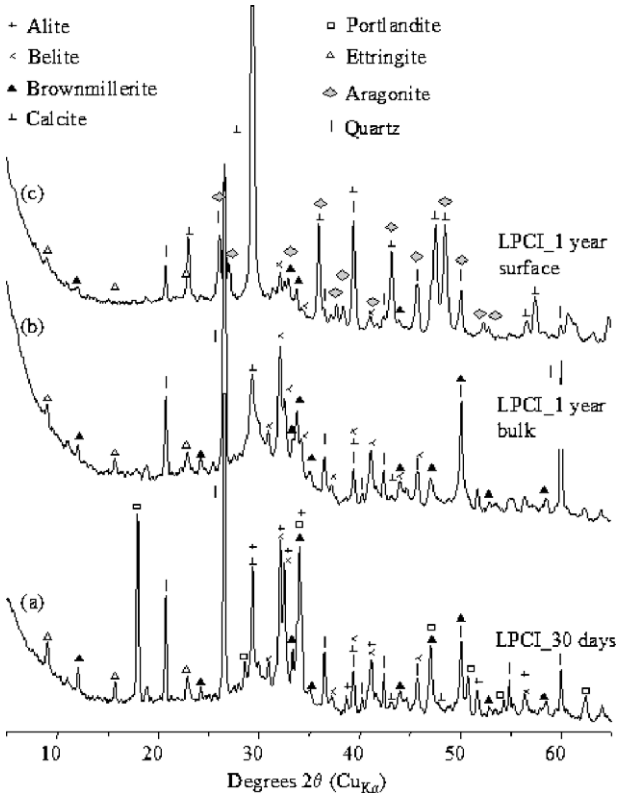

Fig. 1. XRD patterns of samples LPCI hydrated at T=293 K, $p=10^5$ Pa for (a) 30 days and (b, c) one year, CuK_α radiation.

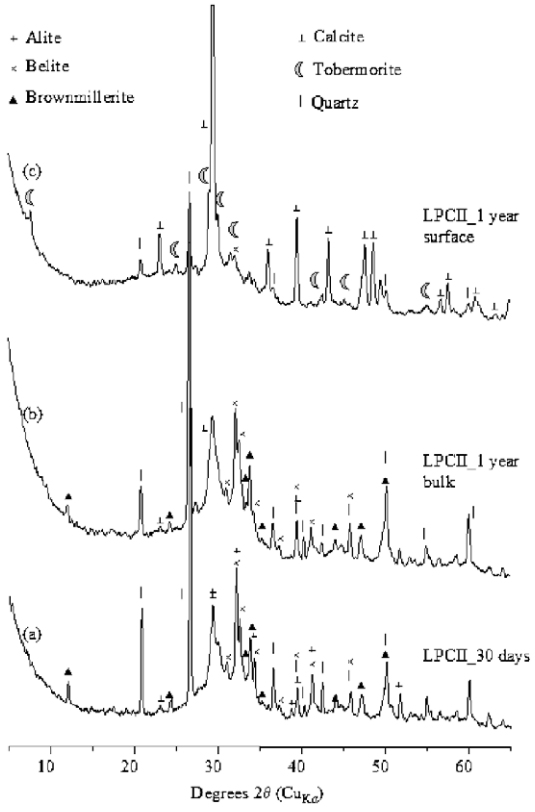

Fig. 2. XRD patterns of samples LPCII hydrated at $T=353$ K, $p=7\times10^6$ Pa for (a) 30 days and (b, c) one year, CuK_α radiation.

phase C_4AF and quartz SiO_2 are found in all samples. The main hydration product common to all samples is the ill crystallized C–S–H, characterized by the diffuse peak at 0.27–0.31 nm (28–33°). We can only notice, as reported in previous work, that elevated temperature impedes the formation of the AF_t phase [10] or induces its decomposition [11]. XRD reveals that portlandite $Ca(OH)_2$ has been consumed before six and one months, respectively in LPCI and LPCII samples. At the surface, the calcite $CaCO_3$ is the main crystalline material (Figs. 1c and 2c) but another polymorph of $CaCO_3$, aragonite, is also present in the LPCI sample. $CaCO_3$ is obtained by dissolution of carbon dioxide in the pore solution of cement paste producing CO_3^{2-} ions, which react with Ca^{2+}. The Ca^{2+} ions required by these reactions are obtained by the dissolution of CH and by lowering the Ca/Si ratio of the C–S–H [12]. 11 Å Tobermorite ($C_5S_6H_5$ approx.) is also identified at the surface in LPCII sample (Fig. 2c) by its reflection at 1.1 nm (8°).

3.2. Magic angle spinning nuclear magnetic resonance spectroscopy

3.2.1. ^{29}Si MAS NMR

Fig. 3a shows the ^{29}Si NMR spectrum of unhydrated class G cement that contains a broad Q^0 component near −71 ppm, which is the sum of alite and belite. As previously proposed by Skibsted et al. [13], the decomposition for the alite and belite components has been determined from the series of inversion-recovery ^{29}Si MAS NMR spectra shown in Fig. 4. This gives relaxation times $T_1=0.043\pm0.002$ s for alite and 0.41 ± 0.04 s for belite in agreement with the observed zero-crossings at the recovery time $t=0.035$ s and $t=0.18$ s for alite and belite, respectively. The ^{29}Si spectrum in Fig. 3c displays a narrow line of Q_s^4 type at −107 ppm and is characteristic of crystalline quartz whereas the broad peak Q_{SF}^4 at −110 ppm in the spectrum for silica fume (Fig. 3b) is characteristic of amorphous SiO_2. All raw materials are still presented in the hydrated cement (Figs. 3d–f and 5). However, the main constituent of the unhydrated cement after one year is belite while the alite has fully reacted. We also observed usual calcium silicate hydrates (C–S–H) except for LPCII_1 year surface sample where silica fume and quartz have disappeared (in fact quartz is present as revealed by XRD patterns but the time delay used in NMR experiments does not permit its quantitative analysis). The resonances lines of C–S–H near −80.2, −82.6, −85.2 and −88.3 were assigned to Q^1, Q^2(1Al) and/or middle tetrahedral of the dreierkette C–S–H chain structure (Q_L^2), Q^2 and bridging tetrahedra connected by hydrogen bond (Q_U^2), respectively (see [3] and references therein).

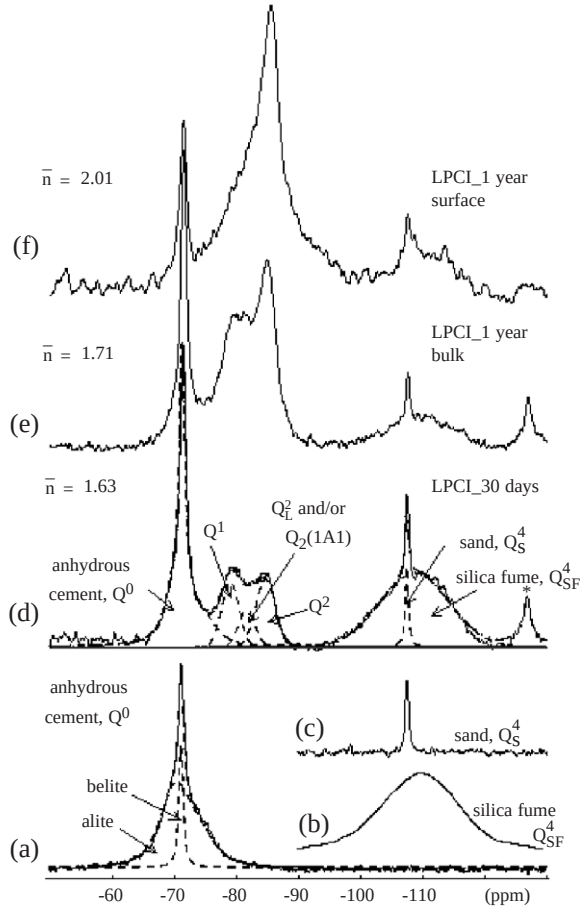

Fig. 3. ^{29}Si MAS NMR spectra of raw materials: (a) unhydrated cement, (b) silica fume, (c) sand and (d, e, f) samples hydrated at $T=293$ K, $p=10^5$ Pa for (d) 30 days and (e, f) one year. The asterisks mark spinning sidebands.

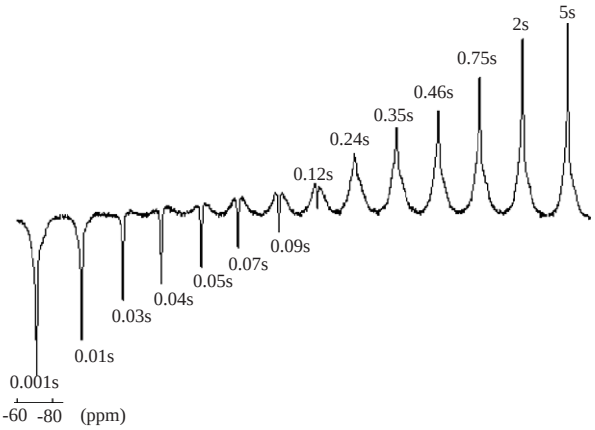

Fig. 4. Inversion-recovery ^{29}Si MAS NMR spectra of an unhydrated class G oilwell cement. The recovery time in seconds is indicated for each spectrum.

The ^{29}Si NMR spectra of the degraded layers after one year show an increase of Q^2 units compared to the bulk sample. Two resonances at about −92 and −96 ppm appear in the LPCII sample (Fig. 5c) where 11 Å Tobermorite has been detected by XRD measurements. According to Wieker et al. [14] synthetic 11 Å Tobermorite exhibits two resonances at −85.7 and −95.7 ppm arising from chain middle group (Q^2) and branching site (Q^3). Furthermore, Komarneni et al. [15] showed that the substitution of aluminium in Tobermorite caused a low field shift of the Q^3 units from −95.7 to −91.5 ppm. Therefore, the observed resonances can be assigned to Al-substituted Tobermorite as follows: $Q^3(1Al)=-92$ ppm and $Q^3(0Al)=-96$ ppm. However, it is difficult to separate the Q^2 sites arising from well crystallised Tobermorite and C–S–H.

The relative proportions of silicon associated with the Q^n units were determined by deconvolution of the spectra and measurement of the area associated with each peak using the dmfit program [16]. We can deduce the average degree of SiO_4 tetrahedra connectivity $\bar{n}$ in the C–S–H and the pozzolanic activity of silica fume PA_{SF} given by:

$$\bar{n} = \frac{Q^1 + 2Q^2 + 3Q^3}{Q^1 + Q^2 + Q^3}$$

$$PA_{SF} = \frac{Q^4_{SF}(t) - Q^4_{SF}(t=0)}{Q^4_{SF}(t=0)}.$$

After 30 days, the average degree of SiO_4 tetrahedra connectivity in the sample LPCI increases with curing time whereas it shows no variation in sample II. The polymerisation of the C–S–H structure increases with temperature and pressure. Such modifications in the hydrates structure may be linked to a change in the Ca/Si ratio. As temperature and pressure increase, the degree of hydration of the anhydrous cement increases as evidenced by the decreasing relative intensity of the Q^0 peak. At the same time, the reaction of silica fume with CH to form C–S–H is activated by temperature and pressure (Fig. 6). This reaction leads to a higher portlandite consumption with temperature and pressure as shown by XRD results. These observations are close to those reported earlier by [17,18] about the reactivity of silica fume blended with Portland cement with curing temperature. The ^{29}Si NMR spectra of the degraded layers after one year show an increase of Q^2 units compared to the bulk sample with the appearance of crystallised 11 Å Tobermorite in the LPCII sample.

3.2.2. ^{27}Al MAS NMR

Chemical analysis performed on sand and silica fume reveals the presence of Al_2O_3 (respectively: 0.56 and 9.33 wt.%). Also, it is important to note that in the cement mix, aluminium originates from anhydrous cement (61.5 mol%), silica fume (36.7 mol%) and sand (1.8 mol%). ^{27}Al NMR spectra of the raw materials used in this study are depicted in Fig. 7a–c and previously described for anhydrous oilwell (Fig. 7c) in Part I. The ^{27}Al NMR spectrum of sand, Fig. 7a, clearly depicts tetrahedrally coordinated Al (57 ppm) whereas the spectrum of silica fume (Fig. 7b) is really broad and difficult to interpret.

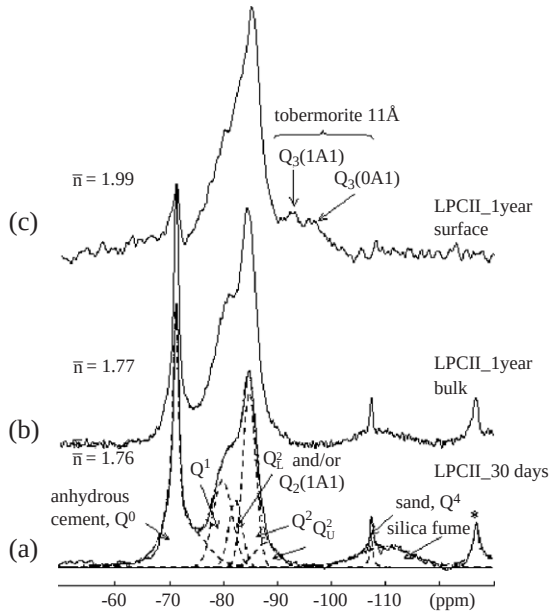

Fig. 5. ^{29}Si MAS NMR spectra of samples hydrated at $T=353$ K, $p=7\times10^6$ Pa for (a) 30 days and (b, c) one year.

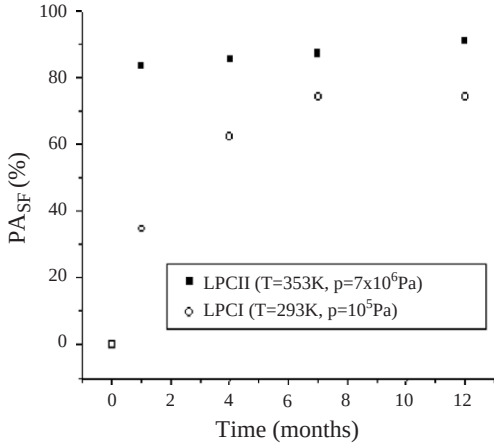

Fig. 6. The pozzolanic activity progress of silica fume PA_{SF} according to ^{29}Si NMR results.

The ^{27}Al NMR spectra of LPC samples are displayed on Figs. 7d–f and 8 and do not reveal the presence of the raw materials. In the LPCI samples, the three main octahedral centre band contributions are identified as AF_t (near 13 ppm), AF_m (near 10 ppm) and a third aluminate phase (near 5 ppm). As previously noticed, AF_m phase is not detected by XRD indicating that the phase is poorly crystalline [12]. The resonance near 5 ppm is assigned to Al^{3+} substituting Ca^{2+} in the octahedral sheet of the C–S–H structure [19] or as a less crystalline alumina phase or a calcium aluminate hydrate including $Al(OH)_6^{3-}$ or $O_xAl(OH)_{6-x}^{(3+x)-}$ octahedra [20]. These phases persist with curing time but the resonance at 5 ppm is only clearly present in the LPCI sample after one year. The hydrated cements also yield signals in the Al (IV) and Al (V) ranges respectively assigned to a less crystalline alumina phase or a calcium aluminate hydrate and Al substituting Si in the C–S–H [13]. After one year, the Al (IV) resonance is still present but more intense in the surface than in the bulk sample. This indicates that chain lengthening observed between the core and surface of the LPCI_1 year surface sample by ^{29}Si NMR, is rather due to incorporation of aluminium in the C–S–H (i.e. Q^2 (1Al) units).

In LPCII samples, there is no or little difference between the spectra of the sample cured 30 days and one year (Fig. 8a–b). Spectra reveal that AF_t phase was absent whereas

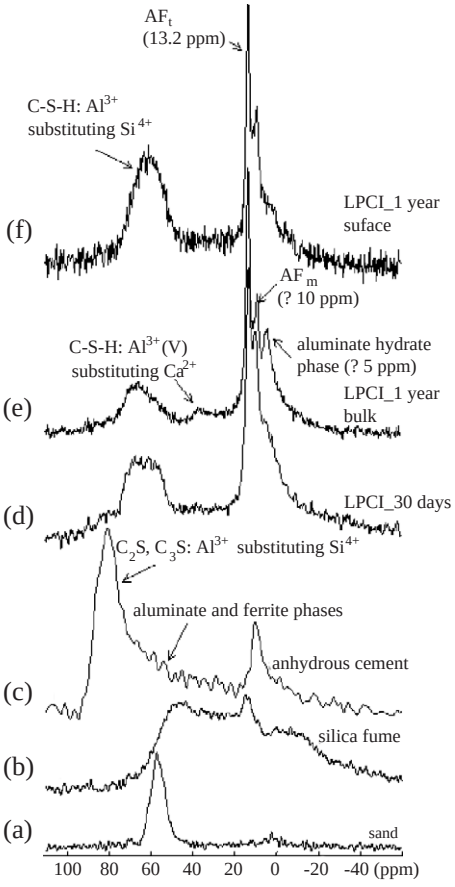

Fig. 7. ^{27}Al MAS NMR spectra of raw materials: (a) sand, (b) silica fume and (c) unhydrated cement and samples hydrated at $T=293$ K, $p=10^5$ Pa for (d) 30 days and (e, f) one year.

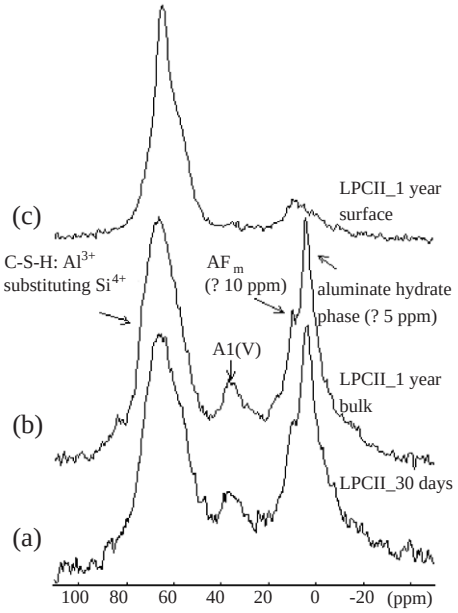

Fig. 8. ^{27}Al MAS NMR spectra of samples hydrated at $T=353$ K, $p=7\times10^6$ Pa for (a) 30 days and (b, c) one year.

AF_m resonance is present but the main contribution of Al (VI) arises from the resonance at 5 ppm not clearly assigned. The resonances attributed to Al (V) and Al (IV) substituting Si in C–S–H are particularly intense in these samples compared to the C [4] and LPCI samples. As previously reported [21] curing at elevated temperatures leads to less formation of AF_t and AF_m phases. Aluminium ion from anhydrous cement but also silica fume and sand will instead increasingly substituted at Si sites in the C–S–H structure and may be at Ca sites. At the surface where Tobermorite has been detected by XRD and ^{29}Si NMR measurements, we observe mainly Al (IV) resonance. Indeed, Komarneni et al. [15] shows that aluminium in Tobermorite structures is only tetrahedrally co-ordinated. The presence of Al in the C–S–H structure and the high temperature and pressure both accelerates Tobermorite formation from C–S–H and as reported in [22] causes it to be stable over a wider temperature range than unsubstituted Tobermorite (i.e. inhibits the conversion to Xonotlite).

4. Conclusion

Low Permeability Class G cement with two curing conditions were analysed by XRD and NMR. Although Fe content of oilwell cement is quite large, reasonable well-defined NMR spectra can be obtained from phases. The sample cured at $T=293$ K, $p=10^5$ Pa during 30 days has a normal mineralogy: unhydrated cement, silica fume, quartz persist and the matrix consists of portlandite, AF_t, AF_m and C–S–H. Before six months, the portlandite has been consumed by silica fume. At the surface, leaching resulted in the formation of calcite by reaction of CO_3^{2-} ions from CO_2 which reacts with Ca^{2+}. The Ca^{2+} ions required by these reactions are obtained by the dissolution of CH and by

lowering the Ca/Si ratio of the C–S–H increasing the polymerisation of the C–S–H structure. In the $T=353$ K, $p=7\times10^6$ Pa mineralogy, AF_t is absent and the average degree of connectivity of the C–S–H structure increased. The reaction of silica fume with CH to form C–S–H is activated by temperature and pressure. The aluminium originating from anhydrous cement, silica fume and sand is highly incorporated in the C–S–H structure and could, with the high temperature and pressure, accelerate Tobermorite formation from C–S–H.

Acknowledgements

The authors would like to thank Institut Français du Pétrole for the permission to publish this paper. They are grateful to Annie Audibert-Hayet for valuable discussions, and Bernadette Rebours, Sylvie Massot, Isabelle Clémençon for their help in XRD measurements.

References

[1] J. Bensted, Special cements, in: P.C. Hewlett (Ed.), LEA's Chemistry of Cement and Concrete, Arnold, London, 1998, pp. 779–835.
[2] C. Noïk, A. Rivereau, C. Vernet, Novel cements materials for high-pressure/high-temperature wells, Paper SPE 50589 Presented at the SPE European Petroleum Conference, The Hague, The Netherlands, October 20–22, 1998.
[3] G. Le Saoût, E. Lécolier, A. Rivereau, H. Zanni, Chemical structure of cement aged at normal and elevated temperatures and pressures: Part I. Class G oilwell cement, Cem. Concr. Res. 36 (2006) 71–78.
[4] G. Le Saoût, E. Lécolier, A. Rivereau, H. Zanni, Micopore size analysis in oil-well cement by proton nuclear relaxation, Magn. Reson. Imaging 23 (2005) 371–373.
[5] H. Zanni, P. Fonollosa, F. Méducin, C. Porteneuve, F. Barberon, J.P. Korb, D. Petit, Nuclear Magnetic Resonance spectroscopy and spin relaxation on cement-based materials-a review, in: G. Grieve, G. Owens (Eds.), Proceedings of the 11th International Congress on the Chemistry of Cement, Durban (South Africa), 2003, pp. 160–170.
[6] G. Le Saoût, E. Lécolier, A. Rivereau, H. Zanni, Study of oilwell cements by solid state NMR, C. R. Chimie 7 (2004) 383–388.
[7] C. Noïk, A. Rivereau, C. Vernet, Slag for cementing a well, in particular an oil well, U.S. Patent n° US 6,332,920 B1 (2001).
[8] P. Richard, M. Cheyrezy, Composition of reactive powder concretes, Cem. Concr. Res. 25 (1995) 1501–1511.
[9] C. Vernet, C. Alonso, C. Andrate, M. Castellote, I. Llorente, A. Hidalgo, A new leaching test based in a running water system to evaluate long-term water resistance of concretes, Adv. Cem. Res. 14 (2002) 157–168.
[10] P. Yan, X. Qin, W. Yang, J. Peng, The semiquantitative determination and morphology of ettringite in pastes containing expansive agent cured in elevated temperature, Cem. Concr. Res. 31 (2001) 1285–1290.
[11] S.L. Colston, P. Barnes, A.C. Jupe, S.D.M. Jacques, C. Hall, P. Livesey, J. Dransfield, N. Meller, G.C. Maitland, An in situ synchrotron energy-dispersive diffraction study of the hydration of oilwell cement systems under high temperature/autoclave conditions up to 130 °C, Cem. Concr. Res. 35 (2005) 2223–2232.
[12] H.F.W. Taylor, Cement Chemistry, Thomas Telford Publishing, London, 1997.
[13] J. Skibsted, H.J. Jakobsen, Characterization of the Calcium Silicate and Aluminate Phases in Anhydrous and Hydrated Portland cements, in: P. Colombet, A.-R. Grimmer, H. Zanni, P. Soozzani (Eds.), Nuclear Magnetic Resonance Spectroscopy of Cement-Based Materials, Springer, Berlin, 1998, pp. 3–45.
[14] W. Wieker, A.-R. Grimmer, A. Winkler, M. Mägi, T. Tarmak, E. Lippmaa, Solid-state high resolution ^{29}Si NMR spectroscopy of synthetic 14 Å, 11 Å and 9 Å Tobermorites, Cem. Concr. Res. 12 (1982) 333–339.
[15] S. Komarneni, R. Roy, D.M. Roy, C.A. Fyfe, G.J. Kennedy, A.A. Bothner-By, J. Dadok, A.S. Chesnick, ^{27}Al and ^{29}Si magic angle spinning nuclear magnetic resonance spectroscopy of Al-substituted tobermorites, J. Mater. Sci. 20 (1985) 4209–4214.
[16] D. Massiot, F. Fayon, M. Capron, I. King, S. Le Calvé, B. Alonso, J.O. Durand, B. Bujoli, Z. Gan, G. Hoatson, Modelling one-and two-dimensional solid-state NMR spectra, Magn. Reson. Chem. 40 (2002) 70–76.
[17] H. Justnes, Kinetics of reaction in cementitious pastes containing Silica Fume as studied by ^{29}Si MAS NMR, in: P. Colombet, A.-R. Grimmer, H. Zanni, P. Soozzani (Eds.), Nuclear Magnetic Resonance Spectroscopy of Cement-Based Materials, Springer, Berlin, 1998, pp. 245–267.
[18] M. Cheyrezy, V. Maret, L. Frouin, Microstructural analysis of RPC (Reactive Powder Concrete), Cem. Concr. Res. 25 (1995) 1491–1500.
[19] P. Faucon, A. Delagrave, J.C. Petit, C. Richet, J.M. Marchand, H. Zanni, Aluminium incorporation in Calcium Silicate Hydrates (C-S-H) depending on Their Ca/Si Ratio, J. Phys. Chem., B 103 (1999) 7796–7802.
[20] M.D. Andersen, H.J. Jakobsen, J. Skibsted, Incorporation of Aluminium in the Silicate Hydrate (C-S-H) of Hydrated Portland cements: A High-Field ^{27}Al and ^{29}Si MAS NMR investigation, Inorg. Chem. 42 (2003) 2280–2287.
[21] K.O. Kjellsen, Heat curing and post heat curing regimes of high-performance concrete: influence on microstructure and C-S-H composition, Cem. Concr. Res. 26 (1996) 295–307.
[22] J.L. Larosa-Thompson, M.W. Grutzeck, C-S-H, tobermorite, and coexisting phases in the system CaO-Al_2O_3-SiO_2-H_2O, World Cem. 1 (1996) 69–74.